REVIEW

Toward the Development of Printable Nanowire Electronics and Sensors

By *Zhiyong Fan, Johnny C. Ho, Toshitake Takahashi, Roie Yerushalmi, Kuniharu Takei, Alexandra C. Ford, Yu-Lun Chueh,* and *Ali Javey**

In recent years, there has been tremendous progress in the research and development of printable electronics on mechanically flexible substrates based on inorganic active components, which provide high performances and stable device operations at low cost. In this regard, various approaches have been developed for the direct transfer or printing of micro- and nanoscale, inorganic semiconductors on substrates. In this review article, we focus on the recent advancements in the large-scale integration of single crystalline, inorganic-nanowire (NW) arrays for electronic and sensor applications, specifically involving the contact printing of NWs at defined locations. We discuss the advantages, limitations, and the state-of-the-art of this technology, and present an integration platform for future printable, heterogeneous-sensor circuitry based on NW parallel arrays.

1. Introduction

Fabrication of printed device and sensor arrays on bendable substrates may enable the development of a wide range of new technologies, including flexible displays,[1–9] radio-frequency (RF) identification tags,[10,11] sensor tapes,[12–16] artificial skin,[17–19] and more. There has been tremendous progress in this field over the past decade, mainly through the exploration of organic materials as the active semiconductor component.[1,3–11,17–19] For instance, all-printed organic electronics have been demonstrated that utilize inkjet printing, screen printing, or stamping of the main device materials, including semiconductors, insulators, and conductors.[20–23] Such methods may have important implications for cost-effective, large-area integration of electronics, and sensors on nonconventional substrates, such as plastic or paper. Additionally, roll-to-roll printing processes for the fabrication of organic devices have been proposed that could further lower their integration cost.[24] Overcoming the relatively poor life-time and the low carrier mobility of organic materials remains a major obstacle in the field.[25–31] There have been tremendous improvements in this regard through systematic studies and design of various organic molecules over the years, and still further optimization may be achieved in the future.[32–38] However, attaining high-performance devices, capable of operating near the performance metrics of inorganic devices (such as Si metal oxide semiconductor field-effect transistors (MOSFETs)) is most likely not feasible with organic channel materials, mainly due to the intrinsic carrier-transport mechanism associated with organic films, and which limits their carrier mobility.[39–42] As a result, while organic electronics are highly attractive for cost-effective, and possibly disposable, electronics, they may have shortcomings for application domains requiring both high performance and low cost. Therefore, developing a new printable electronic-materials technology with enhanced performance and stability is of large interest.[43] Recently, various approaches for utilization of inorganic materials as the active component for high-performance flexible electronics have been demonstrated.[44–47] In one approach, microstructured inorganic semiconductors are first fabricated on bulk wafers by photolithography and etching, and then transferred to mechanically flexible substrates for subsequent device fabrication.[45,48] This method takes advantage of the precision and repeatability of the top-down fabrication to enable a highly viable route to high-performance flexible electronics. In another notable approach, semiconductor nanowires (NWs) have been proposed and demonstrated as versatile building blocks for flexible electronics, involving the chemical vapor deposition (CVD) growth of NWs followed by their transfer and assembly on flexible substrates.[46,49–57] These works demonstrate the feasibility of using inorganic crystalline materials for high-performance printed electronics.[58–61] In this review article, we summarize and discuss the recent advancements toward printed NW-device and -sensor arrays for large-area integration on nonconventional substrates.

In the past decade, synthetic one-dimensional and quasi-one-dimensional nanomaterials have been the focus of vast research efforts due to their size-related intriguing physical properties, and their highly attractive potential as building blocks for nanoscale electronics,[46,54,62–65] optoelectronics,[66–71] chemical/biological sensing,[72–81] and energy conversion/harvesting.[82–88] These nanostructures are typically grown via the "bottom-up"

[*] Prof. A. Javey, Dr. Z. Fan, J. C. Ho, T. Takahashi, Dr. R. Yerushalmi, Dr. K. Takei, A. C. Ford, Dr. Y. L. Chueh
Department of Electrical Engineering and Computer Sciences
Berkeley Sensor and Actuator Center
University of California at Berkeley
Berkeley, CA 94720 (USA)
E-mail: ajavey@berkeley.edu

DOI: 10.1002/adma.200900860

 WILEY InterScience DISCOVER SOMETHING GREAT © 2009 WILEY-VCH Verlag GmbH & Co. KGaA, Weinheim

approaches, which rely on the packing of the atoms/molecules along energetically preferential directions.[89–92] As a result, the grown materials have high crystallinity, which often renders them with superb electrical and optical properties. Specifically, semiconductor NWs are considered as promising materials due to their well-developed synthesis processes and the ability to tailor material properties through shape, size, and atomic-composition control. The as-grown NW materials, however, have random alignment and orientation, unless epitaxial growth is used to enable vertically aligned NW arrays.[92–97] Therefore, developing routes for large-scale assembly of NWs on desired support substrates is needed to further broaden the application spectrum through a hybrid strategy utilizing the "bottom-up" semiconductor materials growth processes with the "top-down" device-fabrication processes.

Significant efforts have been invested in developing generic methods for the assembly of NWs on various substrates. As depicted in Figure 1, some specific approaches include flow-assisted alignment,[51,102–104] Langmuir–Blodgett (LB),[105–107] bubble-blown techniques,[53] and electric-field-directed assembly.[98–101] In all these directions, NWs are first grown and then harvested and suspended in an organic solvent. The NW suspension is then used for the subsequent assembly of NWs on the desired substrate. For example, the flow-assisted alignment technique incorporates microfluidic channels to enable the directional flow of an NW suspension on the surface of the substrate, resulting in the assembly of NWs, but often with low density.[102] On the other hand, the LB approach utilizes the NW–surfactant monolayer on an aqueous subphase to generate an aligned NW layer on the surface of the liquid.[106] The compressed NW layer is then gently transferred to a planar substrate to result in a parallel NW assembly with high degree of alignment and high density. The scalability and uniformity of this approach for large-area NW integration is, however, challenging. Additionally, the blown-bubble method was recently developed, involving the preparation of a homogeneous and stable polymer suspension of NWs.[53] The expansion of the polymer suspension is then performed to form a bubble, and finally the bubble film is transferred to the substrate. Moreover, there have been studies of single or small numbers of NW devices prepared by electric-field-directed assembly, where alternating metal electrodes are buried within the substrate to align NWs by applying an alternative voltage (1 kHz).[98] In this case, NW polarization due to the applied electric field is the driving force in the aligned assembly. While these exciting works have demonstrated the feasibility of parallel-arrayed NW assembly on substrates, they suffer from certain limitations, mainly the scalability, uniformity, and/or the complexity of the processes for use in certain applications.

Ali Javey is an assistant professor of electrical engineering and computer sciences at the University of California-Berkeley and a principal investigator in the Materials Sciences Division at Lawrence Berkeley National Laboratories. After receiving a Ph.D. in chemistry from Stanford University, he joined the faculty at UC Berkeley in 2005. His research interests focus on the integration of synthetic nanomaterials for various technological applications, including high-performance nanoelectronics, flexible circuits and displays, and novel electronic sensors.

To address the need for large-scale and controllable assembly of highly aligned NW parallel arrays, we have developed a contact-printing technology involving the direct transfer of NWs from the growth to the receiver substrates.[49,50,60] This

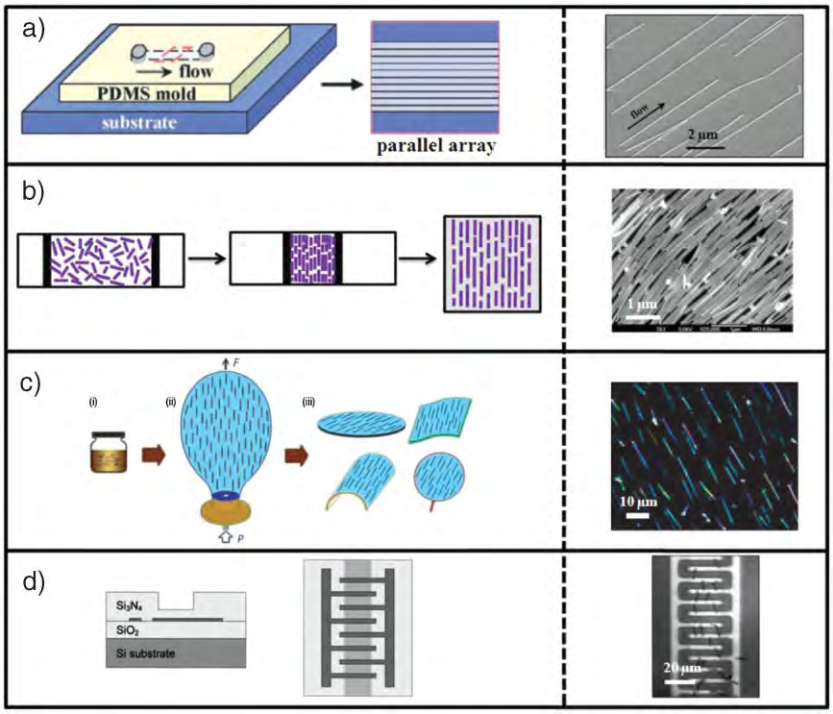

Figure 1. Nanowire-assembly techniques. a) Schematic and the result of flow-assisted NW-assembly method. NWs are flown in microfluidic channels resulting in their aligned assembly. Reproduced with permission from [102]. Copyright 2001 American Association for the Advancement of Science. b) Schematic of LB NW assembly method. Randomly aligned NWs are first floated at the liquid/air interface. Upon lateral mechanical compression, the NWs become well aligned, and form a monolayer that can then be transferred to a planar substrate. Reproduced with permission from [106]. Copyright 2003 American Chemical Society. c) Schematic of blown-bubble NW assembly method. Reproduced with permission from [53]. Copyright 2007 Nature Publishing Group. d) Schematic (left) and optical image (right) of electric field alignment of NWs. The alignment is induced by the polarization of NWs in the applied alternating electric field. Reproduced with permission from [98]. Copyright 2000 American Institute of Physics.

© 2009 WILEY-VCH Verlag GmbH & Co. KGaA, Weinheim

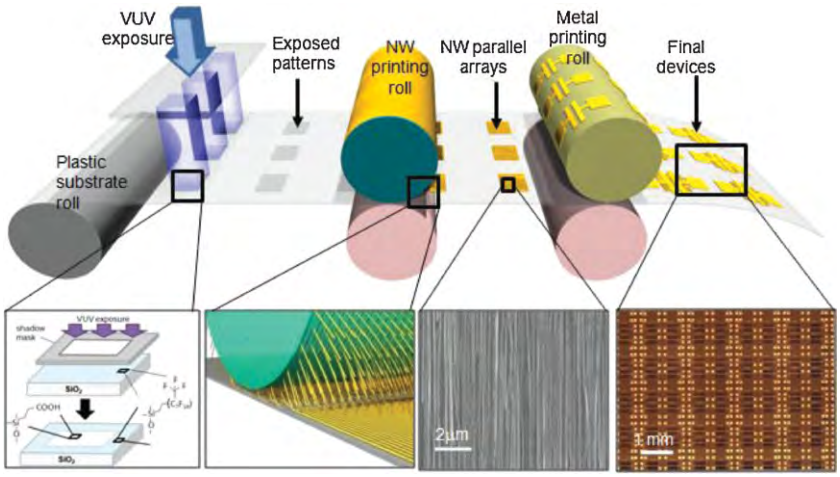

Figure 2. Schematic of an envisioned roll-to-roll printing set-up for NW electronics and sensors fabrication. The process involves fluorinated monolayer patterning of the receiver substrate to define ''sticky'' and ''non-sticky'' regions for the subsequent patterned transfer and assembly of NWs by contact printing. Following the printing of NW active components, devices are fabricated by defining the source/drain and gate electrodes.

technique utilizes shear force to effectively align the NWs, and chemical binding interactions to anchor and transfer the NWs from the growth to the receiver substrate. As a result, highly aligned, parallel arrays of NWs are readily formed on the receiver substrate. The NW contact-printing technology could be an important step toward printed NW sensors and devices on flexible substrates (Fig. 2), which exhibit both low cost and high performances. In such an approach, three main fabrication processes are needed: i) patterning of the receiver substrate to define ''sticky'' and ''non-sticky'' regions for selective NW assembly, ii) contact printing of semiconductor NW arrays as the active channel material, and iii) metal contact and insulator film patterning to complete the device and sensor fabrication. While the third printing step is well established and commonly used by the organic-electronics community,[20,108–111] the first two steps need to be developed for NW systems. In this manuscript, we focus on the recent advancements related to the first two printing steps in route toward the development of an all-printed NW circuitry.

2. Nanowire-Printing Methodology

Semiconductor NWs with desired atomic composition are readily grown by CVD. The diameter of the grown NWs is determined by the size of the metal nanoclusters used as the seeds for the catalytic growth, and can be tuned in the range $d = 10$–500 nm.[112–114] Transmission electron microscopy (TEM) analyses have confirmed the single-crystalline structure of the vapor–liquid–solid (VLS)-grown NWs.[58,61,115–118] The NWs are typically grown vertically on the substrate but with random orientation (for the nonepitaxial growth), therefore resembling a forest, as evident from the scanning electron microscopy (SEM) analysis (Fig. 3a).

Contact printing enables the direct and controllable transfer of NWs from the growth substrate to the desired support (receiver) substrate as highly aligned, parallel arrays (Fig. 3).[49,50,58–60] This method involves the directional sliding of the NW growth substrate (either planar or cylindrical) with randomly aligned NWs on top of a receiver substrate. During this process, NWs are effectively combed (aligned) by the directional shear force, and are eventually detached from the donor substrate as they are anchored by the van der Waals interactions with the surface of the receiver substrate, resulting in the direct transfer of aligned NWs to the receiver substrate.

The growth substrate can be either planar[49,58] or cylindrical.[50] Specifically, the cylindrical growth substrates are used for differential roll printing (DRP) of NWs, which is a highly scalable process.[50] As shown in Figure 3b, the DRP approach is based on the growth of crystalline NWs on a cylindrical substrate (roller) using the VLS process, and then the directional and aligned transfer of the as-grown NWs from the donor roller to a receiver substrate by rolling the roller. This approach minimizes the contact area between the donor and receiver substrates, since the cylindrical donor substrate rolls over the receiver substrate with only a small tangent contact area consisting of fresh NWs at any given time. This is highly beneficial for printing large areas that would otherwise require large planar growth substrates and long contact-sliding distances. In addition, the roller can be repetitively used for the NW growth, which is important for a low-cost roll-to-roll process. Glass, quartz, or stainless-steel tubes with proper outer radius ($r_R \sim 0.25$ inch, limited by the size of the CVD chamber) were used as the cylindrical growth substrates with the NWs grown using similar processing conditions as those used in the synthesis on planar substrates with gold colloids as catalysts. In this case, uniform and dense NW forests are synthesized on the outer surface of the roller. The roller is then connected to a pair of wheels and mounted on rails that guide the directional rolling. During the printing process, the roller is brought in contact with a stationary receiver substrate and rolled at a constant velocity of $\sim$5 mm min^{-1}. The receiver substrate is functionalized with amine-terminated monolayers or thin films of poly-L-lysine. The printing is performed either with or without the application of a lubricant (which will be described in detail in the later section).[50] It was found that the NW assembly is relatively insensitive to the rolling speed, but at high velocities (>20 mm min^{-1}), nonuniform NW printing is attained, arising from the nonconformal contact between the two substrates. The printing outcome, however, highly depends on the roller–receiver substrate pressure. The optimal pressure for the set-up shown in Figure 3b is $\sim$200 g cm^{-2}, which is tuned by the spring underneath the stage. At lower pressures, aligned transfer of NWs is not observed, and at higher pressures, mechanically induced damage to the NWs is observed, resulting in the assembly of short NWs (<1 μm long).

As previously discussed, the application of shear force is essential for the sliding of the NWs on the receiver substrate, which results in their eventual aligned transfer. For planar growth

WILEY InterScience DISCOVER SOMETHING GREAT
© 2009 WILEY-VCH Verlag GmbH & Co. KGaA, Weinheim

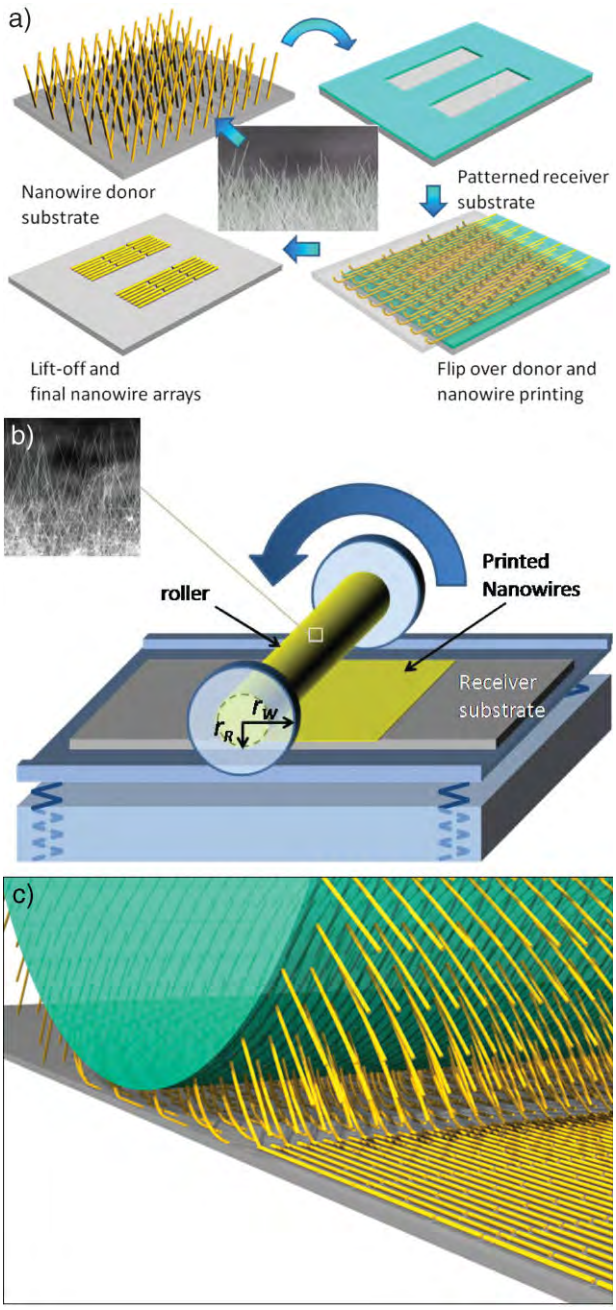

Figure 3. Schematics of NW contact printing involving a) planar and b–c) cylindrical growth (donor) substrates. The SEM images in the insets of a) and b) show that the grown Ge NWs are randomly oriented on the growth substrate, resembling a forest. The NWs are then aligned and transferred to the receiver substrate by application of a directional shear force, resulting in the printing of sub-monolayer NW parallel arrays on the receiver substrate. Images are not to scale.

substrates, the shear force is simply attained by the sliding process. For cylindrical growth substrates (such as DRP process), a mismatch between the roller and wheel radii (r_R and r_W, respectively) is used to result in a linear sliding motion of the roller relative to the stationary receiver substrate in addition to the rolling motion.[50] The relative sliding motion for $r_W \neq r_R$ generates the required shear force for the transfer of aligned NWs to the receiver substrate, without which negligible density with random alignment is observed.[50] This differentiates the NW DRP process from the conventional roll-printing processes where such a mismatch in the radii would be highly undesirable, as it results in the perturbation of the printing patterns. Notably, one rotation of a roller results in a printed region with length equivalent to the circumference of the roller, $2\pi r_W$. Moreover, SEM images of the donor substrate before and after the printing process are investigated, and NWs on the donor substrate are verified to have been effectively combed by the shear force before getting transferred to the receiver substrate. Assuming a NW density of $\sim$5 NW μm^{-2} on the donor substrate and a printed density of $\sim$50 NW/100 μm^2 on the receiver substrate, we estimate that only $\sim$10% of the NWs are transferred during the contact-printing process when the donor and the receiver substrates have the same surface area. Since only $\sim$10% of the grown NWs are transferred from the roller to the receiver substrate after one rotation, in principle, a NW roll can be rotated multiple times before roller replacement is required. However, detailed studies of the printed-NW density and uniformity after multiple rotation cycles are needed in the future.

The ability to assemble crystalline semiconductor NW arrays on various substrate materials is of profound interest for further broadening the potential application domain of this technology. Since the NW printing is performed at ambient temperatures, the process is highly compatible with a wide range of receiver substrates, including those with limited thermal compatibility. For instance, as shown in Figure 4, semiconductor NW arrays were successfully printed on rigid Si (Fig. 4a) and glass (Fig. 4b) substrates, and mechanically bendable paper (Fig. 4b) and plastic (Fig. 4c) substrates.[50] Furthermore, the process is highly generic for various NW materials, including Ge,[49] Si,[49] InAs,[58] and CdSe,[59] and with the entire range of explored diameters (d = 10–100 nm). An essential requirement for the successful printing of aligned NW arrays, however, is to utilize high-quality NW-growth substrates, consisting of high NW density ($\sim$>5 NWs μm^{-1}) with near vertical alignment. When the density of NWs on the growth substrate is relatively low, the grown nonepitaxial NWs exhibit mostly nonvertical orientation, due to the lower steric forces between the NWs, subsequently resulting in poor NW printing outcome (such as poor alignment and density).

2.1. Dynamics of the Printing Process

Understanding the printing dynamics is important to further control the printing-process properties, such as NW density and alignment. Microscopically, the NW printing is composed of three steps: i) NW bending, induced by the application of a normal force, as schematically illustrated in Figure 3a and c; ii) alignment of NWs by the applied shear force; and iii) breakage and transfer of NWs upon anchoring to the receiver substrate through surface chemical and physical interactions. The dominant physical/chemical interactions involved are the van der Waals interactions for NW–receiver substrate and NW–NW.

© 2009 WILEY-VCH Verlag GmbH & Co. KGaA, Weinheim

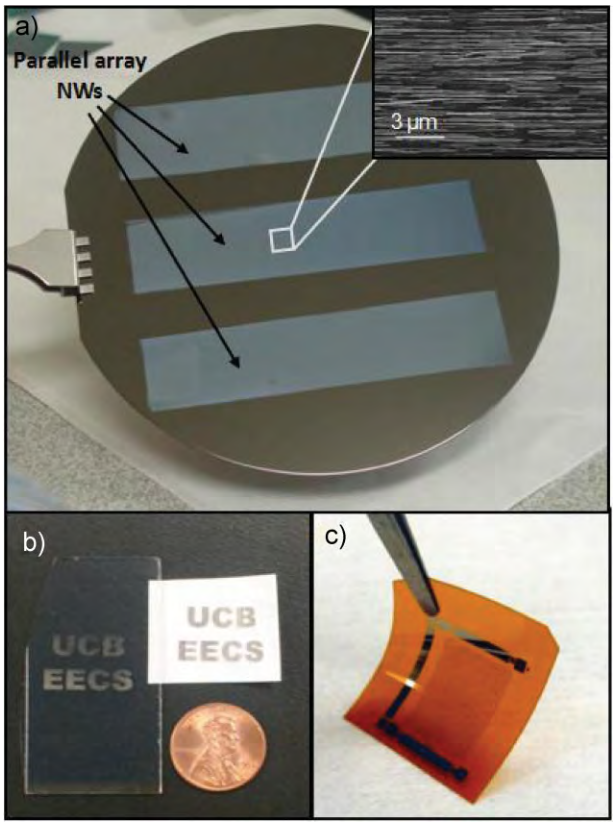

Figure 4. Optical images of Ge-NWs contact printing on a) four inch Si wafer (Reproduced with permission from [49]. Copyright 2008 American Chemical Society); b) glass and photographic paper, and c) mechanically flexible Kapton plastic. Reproduced with permission from [50]. Copyright 2007 American Physical Society.

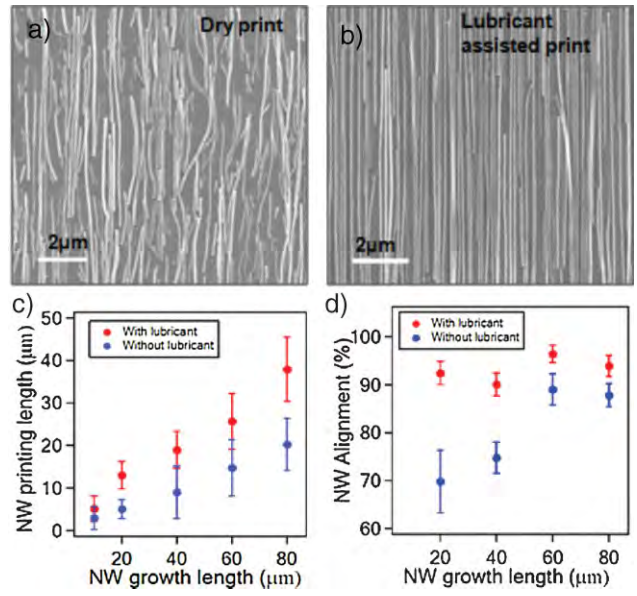

Figure 5. Characterization of printed NW parallel arrays on Si substrates. a,b) SEM images of assembled Ge NWs on Si substrates without and with the use of lubricant (octane/mineral oil, 2:1 v/v) during the printing process, respectively. Application of the lubricant minimizes the mechanical interactions while enhancing the dominant role of surface chemical interactions for controlled NW transfer and assembly with improved NW alignment. Importantly, the NW-printing process is self-limited to the formation of a sub-monolayer due to the weak NW–NW chemical interactions. c,d) Statistical analyses of printed-NW length and alignment as a function of the NW length of the growth substrate. Reproduced with permission from [49]. Copyright 2008 American Chemical Society.

The former interaction favors NW alignment and transfer to the receiver substrate, while the latter interferes with the former to result in poor NW alignment and uncontrollable breakage of NWs due to NW–NW friction. In order to minimize the effects of mechanical friction, a liquid-phase lubricant is applied during the printing process.[49] Figure 5 depicts the importance of lubricant for achieving a controlled NW-transfer outcome with enhanced alignment. Specifically, by applying an octane and mineral oil mixture (2:1 v/v) as the lubricant, the NW contact-printing process can consistently yield highly dense and well-aligned parallel arrays of NWs (Fig. 5b), in clear contrast to the NWs assembled by a "dry" printing process (Fig. 5a).[49]

To quantify the effect of the lubricant on the NW-printing outcome, statistical analyses of the printed-NW length and alignment were performed (Fig. 5c and d).[49] The printed-NW length shows a linear dependence on the initial NW growth length (donor). The average printed NW length, however, is approximately twice higher when a lubricant is applied, as compared to the dry printing. This trend is attributed to the reduction of the undesired mechanical friction by the application of the lubricant. The printed NW alignment was also examined as a function of the NW length. A NW is considered misaligned if it forms $>5^\circ$ angle with respect to the printing direction. As shown in Figure 5d, application of the lubricant results in >90% of printed NWs being well aligned, regardless of the NW growth length. On the other hand, dry printing (without lubricant), results in noticeably worse alignment, especially for the shorter NW growth lengths (Fig. 5d).

The application of lubricant reduces the mechanical friction while enhancing the well-defined and highly tunable chemical interactions between NWs and the receiver substrate. This effect is clearly depicted in Figure 6, where the printing process is conducted on Si/SiO_2 substrates with various surface functionalizations, including siloxane monolayers and poly(L-lysine).[49] Moreover, the printed-NW density for "wet" printing is highly sensitive to the surface functional groups of the receiver substrate. Specifically, for the receiver substrates functionalized with $-CF_3$ terminal groups, which are well known to be highly hydrophobic and "non-sticky," almost no transfer of NWs ($<10^{-3}$ NW μm^{-1}) from the donor to the receiver substrate is observed. On the other hand, an identical printing process on $-NH_2$ and $-N(Me)_3^+$ terminated monolayers resulted in a highly dense NW assembly through the strong surface bonding interactions, approaching $\sim$8 NW μm^{-1}. This almost four orders of magnitude modulation of NW density by controlling the surface chemical interactions is highly desirable for patterned printing of NWs, as described later in this article. Notably, for "dry" printing, the printed-NW density shows a minimal dependence on the surface functional groups, varying only from $\sim$2 to $\sim$7 NW μm^{-1} for fluoro- and amine-terminated surfaces,

WILEY InterScience DISCOVER SOMETHING GREAT
© 2009 WILEY-VCH Verlag GmbH & Co. KGaA, Weinheim

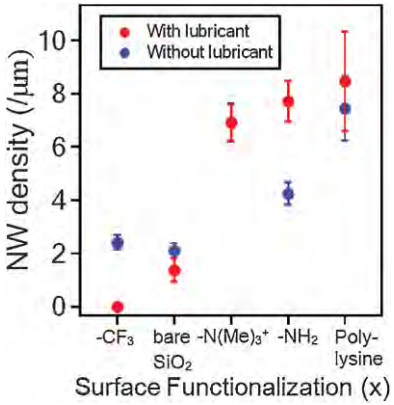

Figure 6. Ge-NW-printing control through the modulation of surface chemical interactions on Si substrates. The density of printed NW arrays on the receiver substrate is shown for different surface functionalization of a Si/SiO_2 (50 nm, thermally grown) receiver substrate. Bare SiO_2 corresponds to using the untreated substrate, while $-CF_3$ [(heptadecafluoro-1,1,2,2-tetrahydrodecyl) dimethylchlorosilane), $-N(Me)_3^+$ (*N*-trimethoxysilylpropyl-*N*,*N*,*N*-trimethylammonium chloride], and $-NH_2$ (3-triethoxysilylpropylamine) correspond to the surface-modified functional groups. Note that, as expected, poly(L-lysine) functionalization results in a larger standard deviation due to the less uniform coverage of the surface by the polymeric thin film, as compared to the molecular monolayers. Reproduced with permission from [49]. Copyright 2008 American Chemical Society.

respectively. This result clearly depicts the important role of the lubricant in the controlled and tunable assembly of NWs. Following the NW assembly, if desired, the organic surface functional group of the receiver substrate can be removed by applying a mild O_2-plasma step (30 W, 30 s) without damaging the inorganic NWs. However, we have not noticed any significant dependence in the electrical and optical properties of the printed NWs as a function of the surface treatment applied to the receiver substrate.

2.2. Patterned Printing

Patterned assembly of semiconductor NWs at predefined locations on the substrate is needed to enable the subsequent device and circuit fabrication. To achieve this goal, receiver substrates with lithographically prepattered photoresist (PR),[49,50] electron-beam resist,[49] or molecular monolayer resist[60] were utilized for the printing process. Figure 7a shows a patterned PR layer (500 nm thick) on a Si/SiO_2 (50 nm) substrate. Following the contact printing, NW parallel arrays are assembled on the PR layer as well as the openings. The subsequent lift-off process in a solvent (for example, acetone) results in the removal of the PR while leaving behind only NWs that were assembled in the prepatterned regions (Fig. 7b). To achieve finer spatial resolution, electron-beam lithography of poly(methyl methacrylate) (PMMA) resist (~100 nm thick) was used to define 200 nm wide openings (Fig. 7c). The patterned substrate was then used as the receiver substrate for NW contact printing. Following the resist lift-off, individual NWs are positioned at predefined sites, demonstrating the ability to control the number of assembled NWs per site by simply tuning the width of the patterned regions in the resist layer. However, as expected, devices based on individual printed NWs show significantly lower yield and higher ON current variation. The NW printing process is, therefore, more applicable for applications requiring parallel arrays of NWs, such as those proposed and described in this article.

To further enhance the scalability of the patterning process and develop practical roll-to-roll printing processes, recently, molecular monolayers were used as the resist layer for achieving pattered NW assemblies.[60] In this process, Si/SiO_2 (50 nm, thermally grown) substrates are chemically reacted with (heptadecafluoro1,1,2,2-tetrahydrodecyl)dimethylchlorosilane (HDF) to form highly stable, fluorinated self-assembled monolayers (SAMs) on the surface. By projecting a very-ultraviolet (VUV, 172 nm, ~25 mW cm^{-2}) light pattern on the surface of the HDF-treated substrate in an oxygen-rich environment, C–F bonds are chemically cleaved and oxidized, resulting in the formation of –COOH and –CHO functional end groups[119,120]

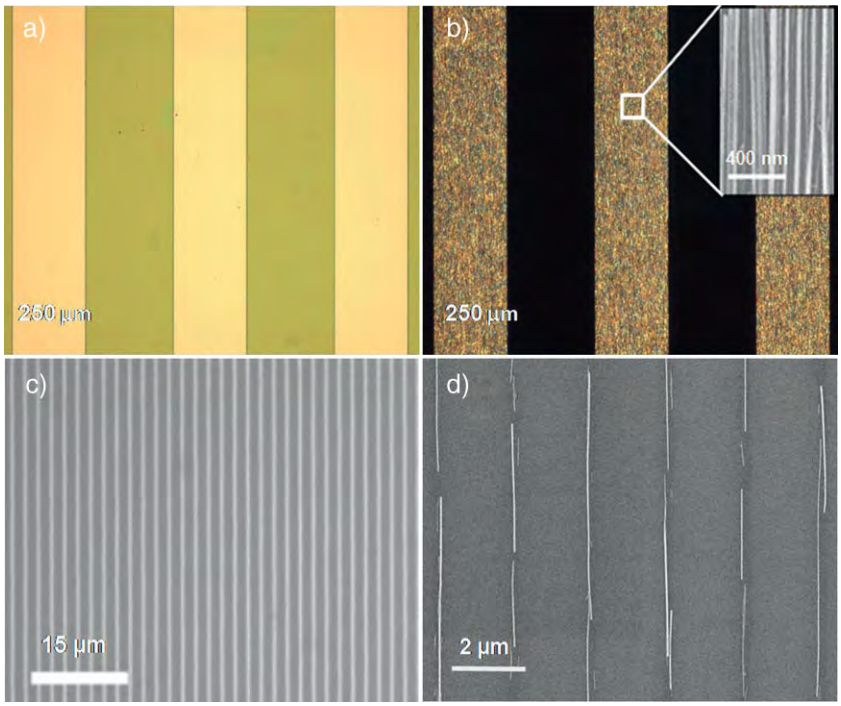

Figure 7. Lithographic patterning of polymer resists for patterned Ge-NW printing on Si substrates. a) Bright-field optical image of a patterned PR layer on a Si/SiO_2 substrate prior to the NW printing process. b) Dark-field optical image of the assembled NWs after the printing and PR lift-off processes. Inset shows the SEM image of the well-aligned NW arrays. c) Bright-field optical image of EBL patterned PMMA layer on a Si/SiO_2 substrate, showing channels with width ~200 nm and 2 μm pitch. d) SEM image of the assembled NWs after NW printing and PMMA lift-off, showing single NW positioning on the substrate. Reproduced with permission from [49]. Copyright 2008 American Chemical Society.

© 2009 WILEY-VCH Verlag GmbH & Co. KGaA, Weinheim

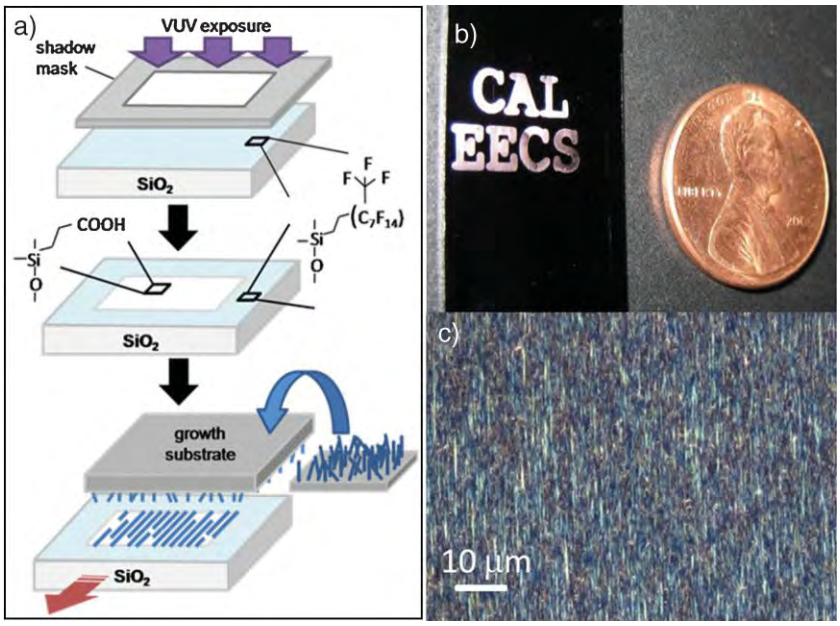

Figure 8. VUV projection patterning of SAM resist for patterned Si-NW printing on Si substrates. a) Schematic of the patterned NW contact printing process using molecular monolayers as the resist. b) Optical image of the patterned Ge NWs printed on a VUV-exposed Si/SiO_2 substrate with the SAM resist. c) High-magnification optical image of the printed NW arrays, showing high NW density with good alignment. Reproduced with permission from [60]. Copyright 2009 American Chemical Society.

(Fig. 8a), as confirmed by X-ray photoelectron spectroscopy (XPS), contact-angle measurements, and ellipsometry. While the fluorinated surfaces are highly non-sticky to NWs, −COOH, and −CHO groups interact strongly with the NW surfaces, most likely through hydrogen bonding with the native oxide layer. As a result, this simple process enables the direct formation of "sticky" and "non-sticky" regions on the receiver substrate (Fig. 8a). During the subsequent NW printing process, NWs only adhere to the VUV exposed regions, resulting in the patterned printing of NWs without the need for a lift-off process. Figure 8b and c shows optical mages of densely packed Ge-NW arrays on the VUV-patterned fluorinated substrate.[60] Clearly, this patterned printing process is quite appealing for all-printed electronics, since the monolayer surface-modification process is in principle a printable process.

2.3. Printing of NW Superstructures

Hierarchical assembly of NW superstructures is of interest for a number of applications, such as those utilizing heterogeneous NW crossbars.[69,121,122] In this regard, NW contact printing was used to conveniently enable large-scale NW crossbar formation through a multistep printing process, as illustrated in Figure 9a.[49] In this process, a layer of parallel NW arrays are pattern printed on the receiver substrate followed by the spin coating of a thin film of PMMA (~40 nm thick) to serve as a buffer layer. A subsequent second patterned printing step is then performed with a 90° rotation in relation to the first step.[49] After photoresist lift-off, the PMMA buffer layer is etched away by a mild O_2-plasma process (60 W, 2 min), therefore resulting in the assembly of large arrays of NW crossbars (Fig. 9b1–2). Importantly, the NW printing process is self-limiting, that is, NWs are rarely found to stack on top of each other during a single printing step. This is due to the weak NW–NW surface chemical interactions, especially when lubricant is applied. As a result, when the two-step cross-printing is performed without the PMMA buffer layer, the second NW printing step does not result in the assembly of NWs in the regions of overlap with the first NW layer (Fig. 9c1–2).

3. Printed-NW Arrays for Electronics, Optoelectronics, and Sensors

In order to investigate the feasibility of the NW contact-printing strategy for device and circuit integration, transistors with different channel widths were fabricated while characterizing their ON current.[49] Figure 10a shows the SEM images of printed core/shell Ge/Si (~15/5 nm) NW arrays that were configured as back-gated FETs by defining Ni/Pd (5/45 nm) source (S) and drain (D) contacts. The channel width ranges from a single NW (~30 nm) up to ~250 μm with a fixed channel length of ~2 μm. It should be noted that only the NWs that directly bridge the S/D electrodes contribute to the current, since NW–NW contact resistance is large and most NWs are not in contact with each other. The average ON current of the fabricated NW FETs linearly scales with the channel width, with a slope of ~5 μA μm^{-1} (Fig. 10b), corresponding to ~5 NW μm^{-1}, as a single Ge/Si NW typically delivers ~1 μA NW^{-1} in the unoptimized back-gated geometry used in this work. This result is indicative of the uniform NW assembly with consistent average density on large-areas, and demonstrates the versatility of the contact-printing process for circuit integration of NW device arrays with tunable ON-state resistance.

3.1. NW Parallel Arrays for Electronics

The ability to print a wide range of NW materials with tunable atomic composition enables the exploration of a spectrum of device structures with desired functionality. For instance, high-electron-mobility (field-effect mobility, $\mu_n > 2000\,cm^2\,V^{-1}\,s^{-1}$) InAs NWs were printed as the channel material for high-performance transistors, capable of delivering high ON currents.[58,61] As shown in Figure 11a, a representative FET consisting of an array of printed InAs NWs with a global back-gate geometry (width ~200 μm, channel length ~3 μm, and SiO_2 gate dielectric ~50 nm) delivers an ON current of ~6 mA at $V_{DS} = 3$ V, which corresponds to ~15 μA per NW (~400 NWs bridging S/D).

© 2009 WILEY-VCH Verlag GmbH & Co. KGaA, Weinheim

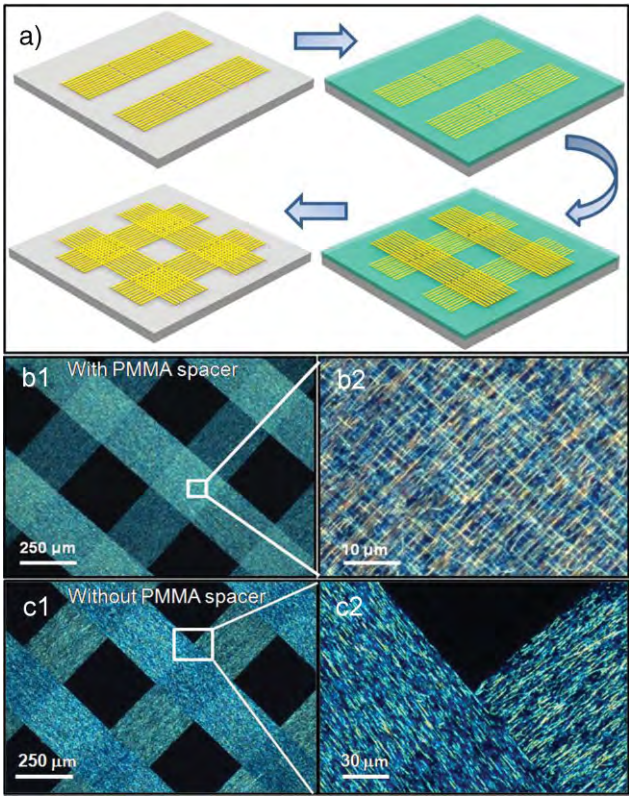

Figure 9. Assembly of Ge-NW superstructures on Si substrates. a) Schematic of a multistep NW printing process for the large-area formation of NW crossbars. b1,b2) Dark-field optical images of SiNW crossbars formed by a two-step printing process with a PMMA buffer layer. Reproduced with permission from [49]. Copyright 2008 American Chemical Society. c1,c2) Dark-field optical images of assembled Si NWs by a two-step printing process, without the use of PMMA buffer layer. Without the PMMA buffer layer, NW crossbars are not formed due to the weak NW–NW chemical surface interactions.

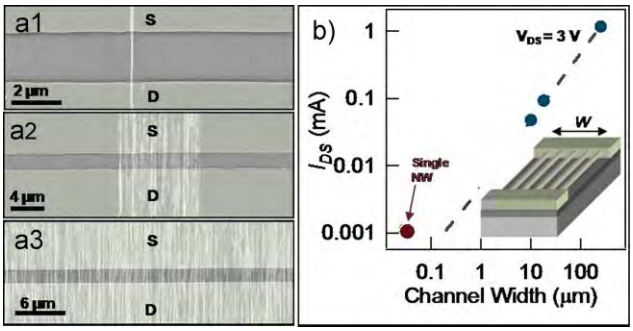

Figure 10. Configuration of NW parallel arrays as the active component of electronic devices on Si substrates. a1–a3) SEM images of back-gated FETs on Si/SiO_2 substrates based on printed Ge/Si core/shell NW arrays with different effective channel widths, defined by the width of the printed NW region. b) The ON currents of NW FETs scale linearly as a function of channel width, indicative of highly uniform NW assembly. Reproduced with permission from [49]. Copyright 2008 American Chemical Society.

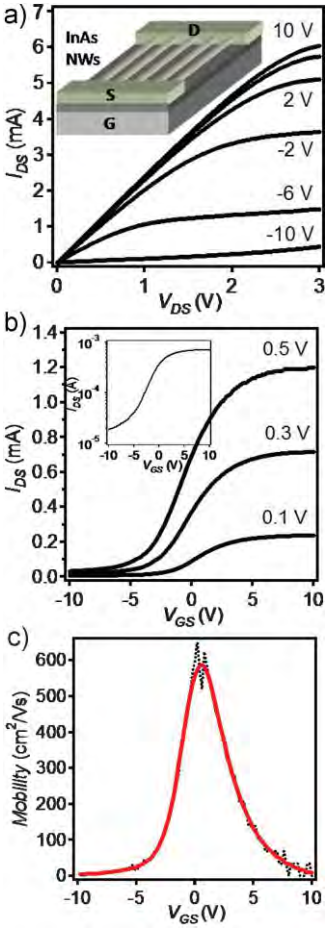

Figure 11. InAs-NW parallel arrays for transistors on Si substrates. a) I_{DS}–V_{DS} and b) linear and log scale (inset) I_{DS} –V_{GS} characteristics of a representative parallel-array InAs NW FET with ~200 µm channel width (~400 NWs bridging S/D electrodes) and ~3 µm channel length. A global back-gate configuration with gate oxide thickness ~50 nm SiO_2 on a p^+ Si substrate is used for this transistor. Reproduced with permission from [58]. Copyright 2008 Trans Tech Publication, Inc. c) Field-effect mobility–V_{GS} curve extracted using the low-bias ($V_{DS} = 0.1$ V) transconductance and the standard square-law model. The curve corresponds to the same array FET with electrical characteristics shown in a) and b).

Importantly, Ohmic metal contacts are readily achieved to the conduction band of InAs NWs, which simplifies the processing while enabling the high ON currents that are observed experimentally.[118] As a result, high-performance printed FETs with potentially high cut-off frequencies may be envisioned in the future by using parallel-array InAs NWs.

Electron mobility is an important figure of merit, since it relates the drift velocity of electrons to an applied electric field, and is used to evaluate FET performance. The transconductance g_m was obtained from the I_{DS}–V_{GS} curve for $V_{DS} = 0.1$V (Fig. 11b), and the standard square law model $\mu_n = (g_m\ L^2)/(C_{ox}\ V_{DS})$ was used to calculate the field-effect mobility μ_n, where L is the channel length and C_{ox} is the gate oxide capacitance. The gate oxide capacitance was approximated by two different methods. As an upper bound estimate for C_{ox} (therefore, a

© 2009 WILEY-VCH Verlag GmbH & Co. KGaA, Weinheim

lower bound estimate for the field-effect mobility), the parallel plate capacitor model $C_{ox} = (\varepsilon\varepsilon_0 A)/d$ was used. Here, ε is the dielectric constant of the oxide (3.9 for SiO_2), ε_0 is the permittivity of free space, A is the channel area (width $\sim$200 μm × length $\sim$3 μm), and d is the thickness of the gate dielectric ($\sim$50 nm). This model gives $C_{ox} = 4.14 \times 10^{-13}$ F and $\mu_n = 92\ cm^2\ V^{-1}\ s^{-1}$ for the parallel-array InAs-NW FETs. A lower bound estimate for C_{ox} (upper bound estimate for the field-effect mobility) was found by multiplying the electrostatically modeled gate oxide capacitance for a single InAs NW ($C_{ox} \sim 0.16 \times 10^{-15}$ F assuming an average NW diameter of $\sim$27 nm and $L = 3$ μm) by the number of NWs in the array FET ($\sim$400). This results in $C_{ox} = 6.49 \times 10^{-14}$ F and $\mu_n = 587\ cm^2\ V^{-1}\ s^{-1}$ (Fig. 11c). Since the parallel-plate capacitor model assumes (incorrectly) that the printed NWs form a continuous sheet across the channel, the actual field-effect mobility of the InAs array FET is likely closer to this upper bound field-effect mobility estimate. The field-effect mobilities reported here are much higher than those of organic semiconductors and amorphous Si, which are typically on the order of $\sim 1\ cm^2\ V^{-1}\ s^{-1}$. This clearly highlights the distinct advantage of using crystalline inorganic materials, such as InAs NWs, as the channel material for high-performance printable electronic devices.

In addition to metal-contacted FETs, printed NW arrays were configured as diodes by using asymmetric metal contacts.[49] Diodes are the most important building blocks of electronics, and are the basis of operation for most devices. Conventional diodes use p- and n- doping of semiconductors to enable the formation of a p–n junction, resulting in the observed rectifying behavior. However, chemical doping[123,124] of the printed NWs on substrates with low thermal budget, such as plastics, is challenging, due to the process temperature limitations. Although advanced processes such as non-equilibrium laser-annealing methods can be used to drive the dopant atoms into the lattice without melting the underlying plastic substrate,[125] such processes are rather difficult, and the large-area uniformity still needs to be further examined. To overcome this limitation, printed Si-NW arrays were configured as Schottky diodes using asymmetric Pd–Al S–D contacts on mechanically flexible Kapton substrates. In this structure, the high-work-function Pd metal forms a low-resistance contact (with small Schottky barriers) to the valence band of the p-SiNWs, whereas low-work-function Al results in a Schottky contact. No thermal annealing is applied after the metalization of the S–D contacts. As a result, Schottky diodes are enabled without the use of dopant profiling (such as p–n junctions). The fabricated diodes exhibit highly rectifying behavior, with $\sim$4 orders of magnitude higher forward than reverse currents (Fig. 12).

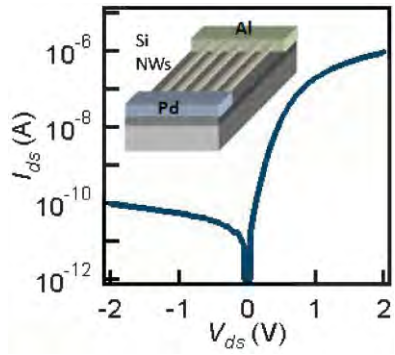

Figure 12. Si-NW parallel array for diodes on Kapton substrates. *I–V* characteristic of a representative Schottky diode fabricated on a printed Si-NW parallel array with channel width $\sim$250 μm and length $\sim$3 μm. Asymmetric Pd and Al contacts, without dopant profiling, are used for the formation of this Schottky diode. Reproduced with permission from [49]. Copyright 2008 American Chemical Society.

3.2. NW Parallel Arrays for Sensors

Besides electronics, NW arrays can be configured as highly responsive sensors. NWs are ideal candidates for chemical and biological sensing, due to i) their chemically active surfaces and large surface-to-volume ratios and ii) their radius being comparable to the Debye screening length, thus resulting in the dominant role of surface electrostatics on the carrier conduction through the entire material.[73,126] To date, researchers have developed a wide range of chemical and biological sensors based on single and arrayed NWs, in some cases with higher detection sensitivity than their thin-film counterparts.[81,127] To demonstrate the potential of NW printing for large-area sensor integration, printed Si-NW arrays were configured as H_2 sensors. As shown in Figure 13a, lightly p-type SiNWs were printed on Si substrates, and two-terminal devices with Ni silicide contacts were fabricated.

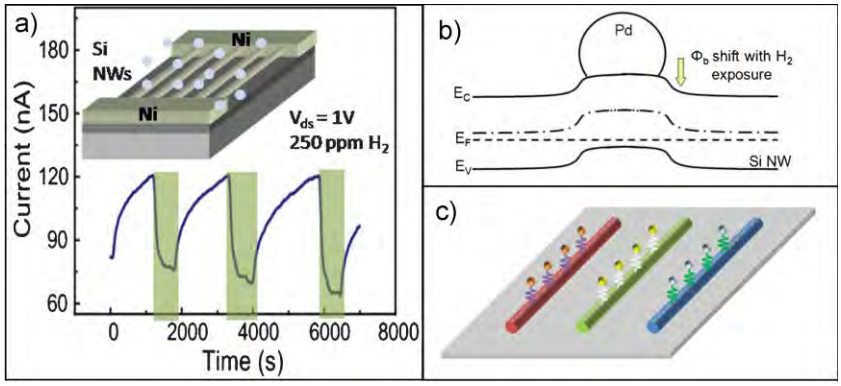

Figure 13. NW parallel arrays for chemical sensors on Si substrates. a) The current output response of a two-terminal device fabricated on printed p-Si NW array with Ni metal contacts as a function of exposure cycles to 250 ppm hydrogen (in dry air). The inset shows the schematic of a sensor device. To induce the H_2 sensitivity, Pd nanoparticles are formed on the surface of Si NWs by thin-film evaporation of Pd. b) Qualitative band diagram, showing the effect of Pd nanoparticles on the local band diagram of Si NWs. Upon H_2 exposure, the work function of Pd nanoparticles is reduced, therefore changing the NW band bending such that the hole-carrier concentration is locally depleted. c) Schematic of an envisioned sensor array, consisting of three different types of NWs sensitive to different chemical species.

© 2009 WILEY-VCH Verlag GmbH & Co. KGaA, Weinheim

To induce sensitivity to H_2, a ~2-nm-thick Pd film was deposited on the printed NW array, resulting in the formation of Pd nanoclusters on the NW surfaces (Fig. 13a). In the absence of hydrogen, the high work function of Pd causes local energy-band bending, which enhances hole transport in the NW channel, as shown in Figure 13b. Upon H_2 exposure, the work function of Pd decreases, resulting in the downwards band bending toward the flat-band condition, thus locally depleting the hole-carrier concentration. Therefore, as shown in Figure 13a, the conductance of the SiNW array shows a strong dependence on the H_2 exposure, even at relatively low concentrations (250 ppm). This concept was previously demonstrated for carbon-nanotube FETs with high sensitivity and low response time arising from the nanoscale dimensions of the Pd clusters, which can undergo rapid absorption and desorption of H_2.[79,128,129]

It is worth noting that the NW-printing method may provide a viable route toward the realization of electronic noses and smart sensors, capable of distinguishing chemical species while determining their concentrations. Such sensors may be envisioned through a large-scale integration of different sensor components (Fig. 13c)[130–132] interfaced with signal-processing functions. To achieve this goal, heterogeneous assembly of NW materials with orthogonal sensitivity to different analytes is needed, which may be achieved in the future through a multistep NW-printing process.

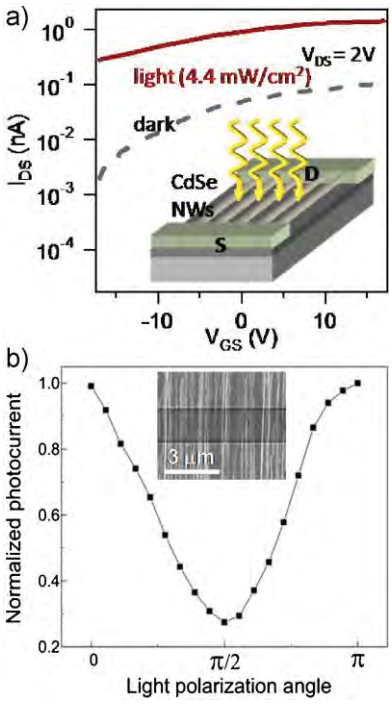

Figure 14. CdSe-NW Schottky devices as highly sensitive optical sensors on Si substrates. a) I_{DS}–V_{GS} characteristics of a back-gated CdSe-NW Schottky photodiode under dark and light illumination (4.4 mW · cm^{-2}) conditions. b) Normalized photocurrent versus angle of the polarization of the incident light, showing strong polarization-dependent light sensing from a well-aligned CdSe-NW array. Reproduced with permission from [59]. Copyright 2008 National Academy of Sciences.

3.3. NW Parallel Arrays for Optoelectronics

Optically active NWs were utilized for various optoelectronics devices. For instance, printed CdSe (direct band gap, $E_g \sim 1.76$ eV)-NW arrays were used for optical sensing.[59] Previous studies have shown that Cd-based and ZnO NWs enable efficient photodetection with significantly higher sensitivities than their bulk counterparts, because of their high surface-area-to-volume ratio that results in higher density of surface states.[133,134] The surface states trap the photogenerated holes, therefore effectively increasing the electron-carrier lifetime and enhancing the observed photocurrent.[133] To configure the printed n-CdSe-NW arrays as photosensors, Schottky-contacted devices were fabricated by contacting the NWs with high-work-function Ni/Pd (5/45 nm) source (S) and drain (D) electrodes, as shown in the schematic of Figure 14a.[59] The electrical characteristic of a representative CdSe-NW Schottky device is presented in Figure 14a, showing a dark resistance $R_{dark} \sim 140$ GΩ due to the high Schottky barriers at the S/D interfaces. These barriers severely limit the carrier injection from the metal into the semiconductor NWs. Upon white-light illumination (halogen light source, 4.4 mW cm^{-2}), the device resistance is dramatically reduced to $R_{light} \sim 2$ GΩ due to the efficient electron/hole photogeneration and field-induced carrier separation in CdSe NWs (Fig. 14a). Importantly, as an optical-sensor element, the NW alignment is extremely critical for uniform response of the devices, and the well-defined polarized sensitivity that arises from the 1D nature of the NWs. For instance, the photoconduction measurements of CdSe-NW parallel arrays exhibit a strong dependence on the illumination polarization, with a minimum photocurrent at 90° and maxima at 0 and 180° (Fig. 14b).[59] This result further confirms the high degree of NW alignment enabled by the contact-printing process.

3.4. All-NW Integrated Sensor Circuitry

The ability to fabricate a wide range of electronic and sensor devices with defined functionalities based on printed NW arrays enables the exploration of heterogeneous NW circuitry with on-chip integration. To examine this feasibility, proof-of-concept circuits were fabricated that incorporate NW sensors and transistors to enable on-chip optical sensing and signal amplification.[59] The layout of an individual all-NW circuit is shown in Figure 15a. Each individual circuit consists of three active device elements: i) an optical nanosensor (NS) based on either a single or parallel array of CdSe NWs, ii) a high-resistance FET (T1) based on parallel arrays of 1–5 Ge/Si core/shell NWs, and iii) a low-resistance buffer FET (T2) with the channel consisting of parallel arrays of ~2000 Ge/Si NWs. The circuitry utilizes T1 to match the output impedance of the NS in a voltage divider configuration in such a way that once the illumination-

© 2009 WILEY-VCH Verlag GmbH & Co. KGaA, Weinheim

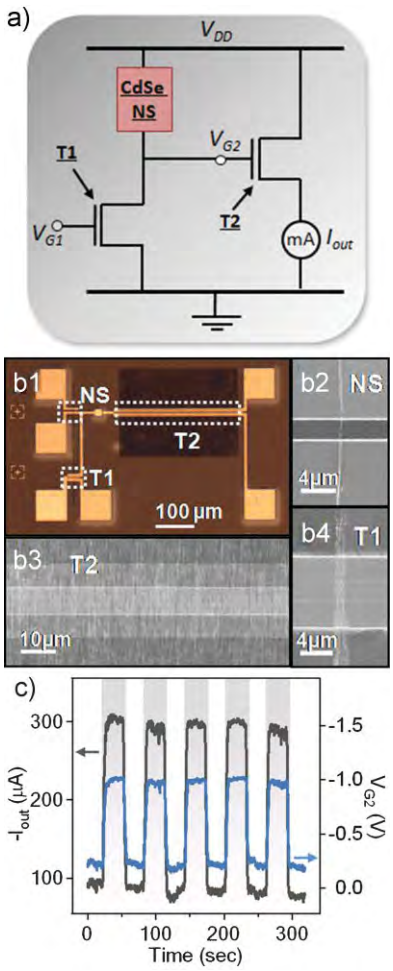

Figure 15. Heterogeneous integration of NWs for sensor circuitry on Si substrates. a) Diagram of a proof-of-concept NW photosensor circuitry, consisting of a CdSe-NW light sensor (NS), an impedance-matching NW transistor (T1), and a buffer transistor (T2). A light signal is detected by the NS and the current output signal is then amplified by the two transistors, which are effectively configured as a voltage divider. b1–b4) Optical and SEM images of an all-NW sensor circuitry with the above mentioned circuit elements. c) The time–domain response of T2 gate voltage, V_{G2}, and circuit output current, I_{out}, for multiple illumination cycles (4.4 mW · cm^{-2}). Reproduced with permission from [59]. Copyright 2008 National Academy of Sciences.

dependent NS current is translated into potential V_{G2}, the output current of T2 is modulated according to its transfer characteristics, resulting in ~5 orders of magnitude amplification of the NS current signal.

In order to fabricate the circuitry, first, highly aligned CdSe and Ge/Si NW arrays were assembled at predefined locations on a Si/SiO_2 (50 nm, thermally grown) substrate using a two-step NW printing process. Then, Ni/Pd S/D electrodes were patterned on NW arrays followed by atomic-layer deposition of a ~8-nm-thick HfO_2 film as the high-κ gate dielectric. Finally, the HfO_2 layer was selectively etched in hydrofluoric acid at the bonding pads and vias, and the top-gate electrodes (Ni/Pd) were patterned on Ge/Si NWs while simultaneously forming the vias between the two metal layers.[59] Figure 15b shows an optical microscopy image of a fabricated circuit and SEM images of each individual component, clearly demonstrating the highly ordered NW positioning and the on-chip integration. The good NW alignment achieved in this study is crucially important for high-performance and highly uniform transistor and sensor arrays, without which significant circuit-to-circuit output variation would be observed. Notably, time-resolved photoresponse measurements were conducted for several illumination cycles, as shown in Figure 15c, showing average dark and light currents of ~80 µA and ~300 µA, respectively. For the circuit-level operation, the operating bias, V_{DD}, was maintained at −3 V for all measurements, while the gate electrode for T1 was biased at $V_{G1} = 3$ V (corresponding to $R_{T1} = 1$–2 GΩ) to match the output impedance of the CdSe NS. The output current is quantitatively consistent with the value that is estimated based on the circuit layout and the electrical properties of the single-device components. For example, the output current of the circuit can be estimated from the transfer characteristics of T2 and the output voltage of the voltage divider, which is also the input to T2. The output of the voltage divider, V_{G2}, can be estimated as $V_{G2} = V_{DD} \times R_{T1}/(R_{T1} + R_{NS})$, corresponding to $V_{G2} \sim -0.02$ V and −1.11 V for dark and light ($R_{NS\text{-dark}} \sim 140$ GΩ and $R_{NS\text{-light}} \sim 2$ GΩ) scenarios. The V_{G2} swing defines the operation regime of T2, and this operation regime corresponds to an output current swing of 87–310 µA, which is in good agreement with the measurements.

To further extend the concept of large-scale heterogeneous integration of parallel-array NW circuitry, large arrays (13 × 20) of the all-NW circuits were fabricated on a chip and utilized as a proof-of-concept imager (Fig. 16a).[59] In this study, each circuit element in the array operates as a single pixel, with an observed functional pixel yield of ~80%. The failure components are mostly due to the materials and processing issues, such as defective NWs, fabrication failures, etc. (Fig. 16b). The functional pixels exhibited a mean photocurrent of ~420 µA, with a standard deviation of ~165 µA. This reasonably small circuit-to-circuit variation arises from the uniformity of the assembled NW arrays, indicative of the potency of the NW printing technology for system integration.

To demonstrate the image-sensing functionality of the all-NW circuit array, a halogen light source was focused and projected onto the center of the matrix (Fig. 16c), and the photoresponse of each individual circuit element was characterized. The output current is measured for each individual working circuit and digitized into a 0–100 scale with "0" and "100" representing the maximum and minimum measured intensities, respectively. The measured intensity level of each circuit was incorporated into a 2D contour plot to create a contrast map, as depicted in Figure 16d. The contrast map clearly illustrates the spatial intensity variation from the center to the outer edge of the circuit matrix, matching the intensity profile of the projected circular light pattern. This work not only demonstrates the NW device integration at an unprecedented scale, but also illustrates and presents a novel platform based on printed NW arrays that may enable a number of technological applications, unattainable with conventional fabrication-processing methods.

© 2009 WILEY-VCH Verlag GmbH & Co. KGaA, Weinheim

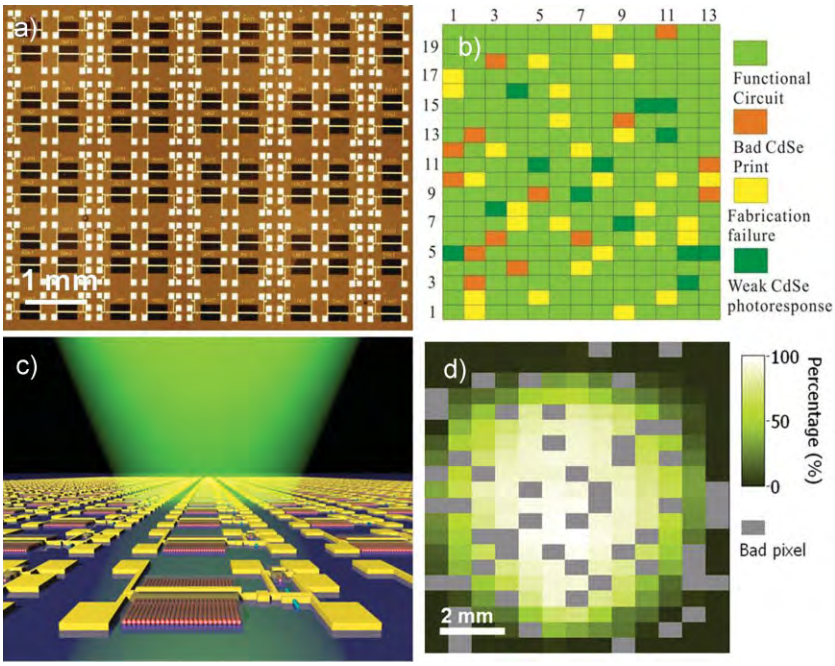

Figure 16. All-NW image sensor on Si Substrates. a) Bright-field optical image of an array of all-NW photosensor circuitry. b) A failure analysis map of the circuit array composed of 20 × 13 individual circuits, showing the distribution of defective circuits. c) A perspective picture showing the imaging function of the circuit array. d) 2D circular-light intensity map imaged by the all-NW sensor arrays, demonstrating a proof-of-concept image sensing. The contrast represents the normalized photocurrent, with the gray pixels representing the defective circuits. Reproduced with permission from [59]. Copyright 2008 National Academy of Sciences.

4. Conclusions

The direct transfer and assembly of parallel-array NWs on various types of substrates by utilizing contact printing may enable the development of an all-printed technology for inorganic electronics and sensors that deliver high performances at low cost. There has been significant progress in controlling the NW contact printing process mostly through the modulation of the nanoscale surface chemical interactions. Specifically, through VUV-directed monolayer patterning of the receiver substrate, ''sticky'' and ''non-sticky'' regions are readily formed, which can then guide the patterned assembly of NWs during the printing process. The printed-NW arrays can be readily configured as a wide range of electronics, optoelectronics, and sensor components with high uniformity over large-areas. Since the printing process is performed at ambient temperatures, the process is compatible with a wide range of substrates, including paper and plastic. More importantly, heterogeneous integration of various NW materials can be achieved through a multistep printing process, therefore enabling the realization of multifunctional circuitry with on-chip integration. While the potency of the printed NW arrays for cost-effective and high-performance devices on non-conventional substrates has already been demonstrated, further work is still needed to demonstrate an all-printed fabrication process for the integrated circuits. Specifically, while a printing process was demonstrated for the NW patterned assembly, to date device fabrication (such as source/drain and gate patterning) has mainly utilized the conventional microfabrication processing. In the future, inkjet or screen printing of the contact materials and gate dielectrics, similar to what is currently being explored for printed organic electronics, need to be incorporated with the NW printing technology for the demonstration of an all-printed NW circuitry.

Acknowledgements

This work was financially supported by DARPA, Intel Corporation, MARCO/MSD Focus Center Research Program, NSF COINS, and Lawrence Berkeley National Laboratory. All fabrication was performed in UC Berkeley Microlab facility. J.C.H acknowledges an Intel graduate fellowship. R.Y. acknowledges a Human Frontiers Science Program fellowship.

Received: March 11, 2009
Revised: April 16, 2009
Published online: June 24, 2009

[1] H. Y. Cheng, C. C. Lee, T. S. Hu, J. C. Ho, *J. Korean Phys. Soc.* **2006**, *48*, S115.
[2] A. B. Chwang, *J. Soc. Inform. Display* **2007**, *15*, 431.
[3] Y. Fujisaki, H. Sato, T. Takei, T. Yamamoto, H. Fujikake, S. Tokito, T. Kurita, *J. Soc. Inform. Display* **2008**, *16*, 1251.
[4] M. Hartney, *Photon. Spectra* **2007**, *41*, 72.
[5] D. Kim, H. Choi, P. Kang, M. Hong, K. Rhie, K. Kim, J. Kim, W. Jang, S. Shin, *Jpn. J. Appl. Phys.* **2008**, *47*, 2195.
[6] P. Mach, S. J. Rodriguez, R. Nortrup, P. Wiltzius, J. A. Rogers, *Appl. Phys. Lett.* **2001**, *78*, 3592.
[7] T. Miteva, V. Yakutkin, G. Nelles, S. Baluschev, *N. J. Phys.* **2008**, *10*, 103002.
[8] S. Takamatsu, M. Nikolou, D. A. Bernards, J. DeFranco, G. G. Malliaras, K. Matsumoto, I. Shimoyama, *Sens. Actuators B* **2008**, *135*, 122.
[9] L. S. Zhou, A. Wanga, S. C. Wu, J. Sun, S. Park, T. N. Jackson, *Appl. Phys. Lett.* **2006**, *88*, 083502.
[10] E. Cantatore, T. C. T. Geuns, G. H. Gelinck, E. van Veenendaal, A. F. A. Gruijthuijsen, L. Schrijnemakers, S. Drews, D. M. de Leeuw, *IEEE J. Solid State Circuits* **2007**, *42*, 84.
[11] V. Subramanian, P. C. Chang, J. B. Lee, S. E. Molesa, S. K. Volkman, *IEEE Trans. Compon. Pack. Technol.* **2005**, *28*, 742.
[12] V. Golovanov, J. L. Solis, V. Lantto, S. Leppavuori, *Sens. Actuators B* **1996**, *34*, 401.
[13] T. Hyodo, T. Mori, A. Kawahara, H. Katsuki, Y. Shimizu, M. Egashira, *Sens. Actuators B* **2001**, *77*, 41.
[14] T. Hyodo, Y. Tominaga, T. Yamaguchi, A. Kawahara, H. Katsuki, Y. Shimizu, M. Egashira, *Electrochemistry* **2003**, *71*, 481.
[15] B. Riviere, J. P. Viricelle, C. Pijolat, *Sens. Actuators B* **2003**, *93*, 531.
[16] H. Zheng, O. T. Sorensen, *Sens. Actuators B* **2000**, *65*, 299.
[17] H. Kawaguchi, T. Someya, T. Sekitani, T. Sakurai, *IEEE J. Solid State Circuits* **2005**, *40*, 177.
[18] T. Someya, T. Sekitani, S. Iba, Y. Kato, H. Kawaguchi, T. Sakurai, *Proc. Natl. Acad. Sci. USA* **2004**, *101*, 9966.
[19] T. Someya, T. Sakurai, *IEEE Int. Electron Dev. Meet.* **2003**, 203.
[20] S. Gamerith, A. Klug, H. Scheiber, U. Scherf, E. Moderegger, E. J. W. List, *Adv. Funct. Mater.* **2007**, *17*, 3111.

© 2009 WILEY-VCH Verlag GmbH & Co. KGaA, Weinheim

[21] S. H. Ko, H. Pan, C. P. Grigoropoulos, C. K. Luscombe, J. M. J. Frechet, D. Poulikakos, *Nanotechnology* **2007**, *18*, 345202.
[22] D. W. Li, L. J. Guo, *J. Phys. D: Appl. Phys.* **2008**, *41*, 105115.
[23] J. H. Cho, J. Lee, Y. Xia, B. Kim, Y. Y. He, M. J. Renn, T. P. Lodge, C. D. Frisbie, *Nat. Mater.* **2008**, *7*, 900.
[24] S. Chun, D. Grudinin, D. Lee, S. H. Kim, G. R. Yi, I. Hwang, *Chem. Mater.* **2009**, *21*, 343.
[25] R. F. Service, *Science* **2000**, *287*, 415.
[26] R. Abbel, M. Woffs, R. A. A. Bovee, J. L. J. van Dongen, X. Lou, O. Henze, W. J. Feast, E. W. Meijer, A. P. H. J. Schenning, *Adv. Mater.* **2009**, *21*, 597.
[27] W. Y. Chou, Y. S. Mai, H. L. Cheng, C. Y. Yeh, C. W. Kuo, F. C. Tang, D. Y. Shu, T. R. Yew, T. C. Wen, *Org. Electr.* **2006**, *7*, 445.
[28] H. Jung, T. Lim, Y. Choi, M. Yi, J. Won, S. Pyo, *Appl. Phys. Lett.* **2008**, *92*, 163504.
[29] R. J. Kline, D. M. DeLongchamp, D. A. Fischer, E. K. Lin, L. J. Richter, M. L. Chabinyc, M. F. Toney, M. Heeney, I. McCulloch, *Macromolecules* **2007**, *40*, 7960.
[30] H. N. Lee, Y. G. Lee, I. H. Ko, E. C. Hwang, S. K. Kang, *Curr. Appl. Phys.* **2008**, *8*, 626.
[31] E. C. P. Smits, S. G. J. Mathijssen, P. A. van Hal, S. Setayesh, T. C. T. Geuns, K. A. H. A. Mutsaers, E. Cantatore, H. J. Wondergem, O. Werzer, R. Resel, M. Kemerink, S. Kirchmeyer, A. M. Muzafarov, S. A. Ponomarenko, B. de Boer, P. W. M. Blom, D. M. de Leeuw, *Nature* **2008**, *455*, 956.
[32] N. Tessler, D. J. Pinner, V. Cleave, D. S. Thomas, G. Yahioglu, P. Le Barny, R. H. Friend, *Appl. Phys. Lett.* **1999**, *74*, 2764.
[33] Y. Jang, D. H. Kim, Y. D. Park, J. H. Cho, M. Hwang, K. W. Cho, *Appl. Phys. Lett.* **2006**, *88*, 072101.
[34] T. W. Lee, J. H. Shin, I. N. Kang, S. Y. Lee, *Adv. Mater.* **2007**, *19*, 2702.
[35] S. Ono, S. Seki, R. Hirahara, Y. Tominari, J. Takeya, *Appl. Phys. Lett.* **2008**, *92*, 103313.
[36] H. Yan, Z. H. Chen, Y. Zheng, C. Newman, J. R. Quinn, F. Dotz, M. Kastler, A. Facchetti, *Nature* **2009**, *457*, 679.
[37] J. Smith, R. Hamilton, M. Heeney, D. M. de Leeuw, E. Cantatore, J. E. Anthony, I. McCulloch, D. D. C. Bradley, T. D. Anthopoulos, *Appl. Phys. Lett.* **2008**, *93*, 253301.
[38] Q. Zhao, T. H. Kim, J. W. Park, S. O. Kim, S. O. Jung, J. W. Kim, T. Ahn, Y. H. Kim, M. H. Yi, S. K. Kwon, *Adv. Mater.* **2008**, *20*, 4868.
[39] M. Kastler, W. Pisula, F. Laquai, A. Kumar, R. J. Davies, S. Baluschev, M. C. Garcia-Gutierrez, D. Wasserfallen, H. J. Butt, C. Riekel, G. Wegner, K. Mullen, *Adv. Mater.* **2006**, *18*, 2255.
[40] S. P. Singh, P. Sonar, A. Sellinger, A. Dodabalapur, *Appl. Phys. Lett.* **2009**, *94*, 013308.
[41] P. T. Wu, T. Bull, F. S. Kim, C. K. Luscombe, S. A. Jenekhe, *Macromolecules* **2009**, *42*, 671.
[42] F. P. Zhang, M. Funahashi, N. Tamaoki, *Org. Electr.* **2009**, *10*, 73.
[43] R. H. Reuss, B. R. Chalamala, A. Moussessian, M. G. Kane, A. Kumar, D. C. Zhang, J. A. Rogers, M. Hatalis, D. Temple, G. Moddel, B. J. Eliasson, M. J. Estes, J. Kunze, E. S. Handy, E. S. Harmon, D. B. Salzman, J. M. Woodall, M. A. Alam, J. Y. Murthy, S. C. Jacobsen, M. Olivier, D. Markus, P. M. Campbell, E. Snow, *Proc. IEEE* **2005**, *93*, 1239.
[44] J. Yoon, A. J. Baca, S. Park, P. Elvikis, J. B. Geddes, L. Li, R. H. Kim, J. Xiao, S. Wang, T. Kim, M. J. Motala, B. Y. Ahn, E. B. Duoss, J. A. Lewis, R. G. Nuzzo, P. M. Ferreir, Y. Huang, A. Rockett, J. A. Rogers, *Nat. Mater.* **2008**, *7*, 907.
[45] Y. G. Sun, H. S. Kim, E. Menard, S. Kim, I. Adesida, J. A. Rogers, *Small* **2006**, *2*, 1330.
[46] A. Javey, S. Nam, R. S. Friedman, H. Yan, C. M. Lieber, *Nano Lett.* **2007**, *7*, 773.
[47] K. J. Lee, M. J. Motala, M. A. Meitl, W. R. Childs, E. Menard, A. K. Shim, J. A. Rogers, R. G. Nuzzo, *Adv. Mater.* **2005**, *17*, 2332.
[48] M. C. Mcalpine, H. Ahmad, D. Wang, J. R. Heath, *Nat. Mater.* **2007**, *6*, 379.
[49] Z. Fan, J. C. Ho, Z. A. Jacobson, R. Yerushalmi, R. L. Alley, H. Razavi, A. Javey, *Nano Lett.* **2008**, *8*, 20.
[50] R. Yerushalmi, Z. A. Jacobson, J. C. Ho, Z. Fan, A. Javey, *Appl. Phys. Lett.* **2007**, *91*, 203104.
[51] X. F. Duan, C. M. Niu, V. Sahi, J. Chen, J. W. Parce, S. Empedocles, J. L. Goldman, *Nature* **2003**, *425*, 274.
[52] S. J. Kang, C. Kocabas, T. Ozel, M. Shim, N. Pimparkar, M. A. Alam, S. V. Rotkin, J. A. Rogers, *Nat. Nanotechnol.* **2007**, *2*, 230.
[53] G. Yu, A. Cao, C. M. Lieber, *Nat. Nanotechnol.* **2007**, *2*, 372.
[54] M. C. Mcalpine, R. S. Friedman, C. M. Lieber, *Proc. IEEE* **2005**, *93*, 1357.
[55] B. P. Timko, T. Cohen-Karni, G. Yu, Q. Qing, B. Tian, C. M. Lieber, *Nano Lett.* **2009**, *9*, 914.
[56] A. J. Baca, J. H. Ahn, Y. Sun, M. A. Meitl, E. Menard, H. S. Kim, W. M. Choi, D. H. Kim, Y. Huang, J. A. Rogers, *Angew. Chem. Int. Ed.* **2008**, *47*, 5524.
[57] X. F. Duan, *IEEE Trans. Electron Dev.* **2008**, *55*, 3056.
[58] A. C. Ford, J. C. Ho, Z. Fan, O. Ergen, V. Altoe, S. Aloni, H. Razavi, A. Javey, *Nano Res.* **2008**, *1*, 32.
[59] Z. Fan, J. C. Ho, Z. A. Jacobson, H. Razavi, A. Javey, *Proc. Natl. Acad. Sci. USA* **2008**, *105*, 11066.
[60] T. Takahashi, K. Takei, J. C. Ho, Y. L. Chueh, Z. Fan, A. Javey, *J. Am. Chem. Soc.* **2009**, *131*, 2102.
[61] A. C. Ford, J. C. Ho, Y. L. Chueh, Y. C. Tseng, Z. Y. Fan, J. Guo, J. Bokor, A. Javey, *Nano Lett.* **2009**, *9*, 360.
[62] R. S. Friedman, M. C. McAlpine, D. S. Ricketts, D. Ham, C. M. Lieber, *Nature* **2005**, *434*, 1085.
[63] J. Xiang, W. Lu, Y. J. Hu, Y. Wu, H. Yan, C. M. Lieber, *Nature* **2006**, *441*, 489.
[64] A. Javey, *ACS Nano* **2008**, *2*, 1329.
[65] A. Javey, H. Kim, M. Brink, Q. Wang, A. Ural, J. Guo, P. McIntyre, P. McEuen, M. Lundstrom, H. J. Dai, *Nat. Mater.* **2002**, *1*, 241.
[66] J. F. Wang, M. S. Gudiksen, X. F. Duan, Y. Cui, C. M. Lieber, *Science* **2001**, *293*, 1455.
[67] Z. H. Zhong, F. Qian, D. L. Wang, C. M. Lieber, *Nano Lett.* **2003**, *3*, 343.
[68] F. Qian, S. Gradecak, Y. Li, C. Y. Wen, C. M. Lieber, *Nano Lett.* **2005**, *5*, 2287.
[69] Y. Huang, X. F. Duan, C. M. Lieber, *Small* **2005**, *1*, 142.
[70] A. B. Greytak, C. J. Barrelet, Y. Li, C. M. Lieber, *Appl. Phys. Lett.* **2005**, *87*, 151103.
[71] Z. Y. Fan, P. C. Chang, J. G. Lu, E. C. Walter, R. M. Penner, C. H. Lin, H. P. Lee, *Appl. Phys. Lett.* **2004**, *85*, 6128.
[72] Z. Y. Fan, D. W. Wang, P. C. Chang, W. Y. Tseng, J. G. Lu, *Appl. Phys. Lett.* **2004**, *85*, 5923.
[73] Z. Y. Fan, J. G. Lu, *Appl. Phys. Lett.* **2005**, *86*, 123510.
[74] Y. Cui, Q. Q. Wei, H. K. Park, C. M. Lieber, *Science* **2001**, *293*, 1289.
[75] F. Patolsky, G. F. Zheng, O. Hayden, M. Lakadamyali, X. W. Zhuang, C. M. Lieber, *Proc. Natl. Acad. Sci. USA* **2004**, *101*, 14017.
[76] J. Hahm, C. M. Lieber, *Nano Lett.* **2004**, *4*, 51.
[77] G. F. Zheng, F. Patolsky, Y. Cui, W. U. Wang, C. M. Lieber, *Nat. Biotechnol.* **2005**, *23*, 1294.
[78] W. U. Wang, C. Chen, K. H. Lin, Y. Fang, C. M. Lieber, *Proc. Natl. Acad. Sci. USA* **2005**, *102*, 3208.
[79] J. Kong, N. R. Franklin, C. W. Zhou, M. G. Chapline, S. Peng, K. J. Cho, H. J. Dai, *Science* **2000**, *287*, 622.
[80] Q. F. Pengfei, O. Vermesh, M. Grecu, A. Javey, O. Wang, H. J. Dai, S. Peng, K. J. Cho, *Nano Lett.* **2003**, *3*, 347.
[81] D. H. Zhang, Z. Q. Liu, C. Li, T. Tang, X. L. Liu, S. Han, B. Lei, C. W. Zhou, *Nano Lett.* **2004**, *4*, 1919.
[82] T. J. Kempa, B. Tian, D. R. Kim, J. Hu, X. Zheng, C. M. Lieber, *Nano Lett.* **2008**, *8*, 3456.
[83] C. K. Chan, H. L. Peng, G. Liu, K. McIlwrath, X. F. Zhang, R. A. Huggins, Y. Cui, *Nat. Nanotechnol.* **2008**, *3*, 31.
[84] L. Tsakalakos, *Mater. Sci. Eng. R. Rep.* **2008**, *62*, 175.
[85] M. Law, L. E. Greene, J. C. Johnson, R. Saykally, P. D. Yang, *Nat. Mater.* **2005**, *4*, 455.
[86] X. D. Wang, J. H. Song, J. Liu, Z. L. Wang, *Science* **2007**, *316*, 102.

© 2009 WILEY-VCH Verlag GmbH & Co. KGaA, Weinheim

[87] A. I. Hochbaum, R. K. Chen, R. D. Delgado, W. J. Liang, E. C. Garnett, M. Najarian, A. Majumdar, P. D. Yang, *Nature* **2008**, *451*, 163.
[88] Y. B. Tang, Z. H. Chen, H. S. Song, C. S. Lee, H. T. Cong, H. M. Cheng, W. J. Zhang, I. Bello, S. T. Lee, *Nano Lett.* **2008**, *8*, 4191.
[89] E. I. Givargizov, *J. Cryst. Growth* **1975**, *31*, 20.
[90] V. Gottschalch, G. Wagner, J. Bauer, H. Paetzelt, M. Shirnow, *J. Cryst. Growth* **2008**, *310*, 5123.
[91] M. T. Borgstrom, G. Immink, B. Ketelaars, R. Algra, E. P. A. M. Bakkers, *Nat. Nanotechnol.* **2007**, *2*, 541.
[92] Y. W. Wang, V. Schmidt, S. Senz, U. Gosele, *Nat. Nanotechnol.* **2006**, *1*, 186.
[93] T. Shimizu, T. Xie, J. Nishikawa, S. Shingubara, S. Senz, U. Gosele, *Adv. Mater.* **2007**, *19*, 917.
[94] Y. K. Tseng, C. T. Chia, C. Y. Tsay, L. J. Lin, H. M. Cheng, C. Y. Kwo, I. C. Chen, *J. Electrochem. Soc.* **2005**, *152*, G95.
[95] E. P. A. M. Bakkers, J. A. Van Dam, S. De Franceschi, L. P. Kouwenhoven, M. Kaiser, M. Verheijen, H. Wondergem, P. Van der Sluis, *Nat. Mater.* **2004**, *3*, 769.
[96] T. Martensson, C. P. T. Svensson, B. A. Wacaser, M. W. Larsson, W. Seifert, K. Deppert, A. Gustafsson, L. R. Wallenberg, L. Samuelson, *Nano Lett.* **2004**, *4*, 1987.
[97] P. Nguyen, H. T. Ng, J. Kong, A. M. Cassell, R. Quinn, J. Li, J. Han, M. McNeil, M. Meyyappan, *Nano Lett.* **2003**, *3*, 925.
[98] P. A. Smith, C. D. Nordquist, T. N. Jackson, T. S. Mayer, B. R. Martin, J. Mbindyo, T. E. Mallouk, *Appl. Phys. Lett.* **2000**, *77*, 1399.
[99] L. F. Dong, J. Bush, V. Chirayos, R. Solanki, J. Jiao, *Nano Lett.* **2005**, *5*, 2112.
[100] Y. Cao, W. Liu, J. L. Sun, Y. P. Han, J. H. Zhang, S. Liu, H. S. Sun, J. H. Guo, *Nanotechnology* **2006**, *17*, 2378.
[101] O. Englander, D. Christensen, J. Kim, L. W. Lin, S. J. S. Morris, *Nano Lett.* **2005**, *5*, 705.
[102] Y. Huang, X. F. Duan, Q. Q. Wei, C. M. Lieber, *Science* **2001**, *291*, 630.
[103] C. Yan, T. Zhang, P. S. Lee, *Appl. Phys. A: Mater. Sci. Process.* **2009**, *94*, 763.
[104] C. Y. Geng, Y. Jiang, Y. Yao, X. M. Meng, J. A. Zapien, C. S. Lee, Y. Lifshitz, S. T. Lee, *Adv. Funct. Mater.* **2004**, *14*, 589.
[105] S. Jin, D. M. Whang, M. C. McAlpine, R. S. Friedman, Y. Wu, C. M. Lieber, *Nano Lett.* **2004**, *4*, 915.
[106] A. Tao, F. Kim, C. Hess, J. Goldberger, R. R. He, Y. G. Sun, Y. N. Xia, P. D. Yang, *Nano Lett.* **2003**, *3*, 1229.
[107] X. L. Li, L. Zhang, X. R. Wang, I. Shimoyama, X. M. Sun, W. S. Seo, H. J. Dai, *J. Am. Chem. Soc.* **2007**, *129*, 4890.
[108] C. Kim, Z. Wang, H. Choi, Y. Ha, A. Facchetti, T. J. Marks, *J. Am. Chem. Soc.* **2008**, *130*, 6867.
[109] T. Sekitani, Y. Noguchi, U. Zschieschang, H. Klauk, T. Someya, *Proc. Natl. Acad. Sci. USA* **2008**, *105*, 4976.
[110] Z. C. Liu, Y. Su, K. Varahramyan, *Thin Solid Films* **2005**, *478*, 275.
[111] R. Parashkov, E. Becker, G. Ginev, T. Riedl, H. H. Johannes, W. Kowalsky, *J. Appl. Phys.* **2004**, *95*, 1594.
[112] Y. Cui, L. J. Lauhon, M. S. Gudiksen, J. F. Wang, C. M. Lieber, *Appl. Phys. Lett.* **2001**, *78*, 2214.
[113] X. Zhang, K. Lew, P. Nimmatoori, J. M. Redwing, E. C. Dickey, *Nano Lett.* **2007**, *7*, 3241.
[114] N. Wang, Y. Cai, R. Q. Zhang, *Mater. Sci. Eng. Res. Rep.* **2008**, *60*, 1.
[115] Y. Cui, Z. H. Zhong, D. L. Wang, W. U. Wang, C. M. Lieber, *Nano Lett.* **2003**, *3*, 149.
[116] A. B. Greytak, L. J. Lauhon, M. S. Gudiksen, C. M. Lieber, *Appl. Phys. Lett.* **2004**, *84*, 4176.
[117] W. Lu, J. Xiang, B. P. Timko, Y. Wu, C. M. Lieber, *Proc. Natl. Acad. Sci. USA* **2005**, *102*, 10046.
[118] Y. L. Chueh, A. C. Ford, J. C. Ho, Z. A. Jacobson, Z. Fan, C. Y. Chen, L. J. Chou, A. Javey, *Nano Lett.* **2008**, *8*, 4528.
[119] Y. J. Kim, K. H. Lee, H. Sano, J. Han, T. Ichii, K. Murase, H. Sugimura, *Jpn. J. Appl. Phys.* **2008**, *47*, 307.
[120] S. L. Brandow, M. S. Chen, R. Aggarwal, C. S. Dulcey, J. M. Calvert, W. J. Dressick, *Langmuir* **1999**, *15*, 5429.
[121] G. Y. Jung, E. Johnston-Halperin, W. Wu, Z. N. Yu, S. Y. Wang, W. M. Tong, Z. Y. Li, J. E. Green, B. A. Sheriff, A. Boukai, Y. Bunimovich, J. R. Heath, R. S. Williams, *Nano Lett.* **2006**, *6*, 351.
[122] D. Whang, S. Jin, Y. Wu, C. M. Lieber, *Nano Lett.* **2003**, *3*, 1255.
[123] J. C. Ho, R. Yerushalmi, Z. A. Jacobson, Z. Fan, R. L. Alley, A. Javey, *Nat. Mater.* **2008**, *7*, 62.
[124] J. C. Ho, R. Yerushalmi, G. Smith, P. Majhi, J. Bennett, J. Halim, V. N. Faifer, A. Javey, *Nano Lett.* **2009**, *9*, 725.
[125] N. Misra, C. P. Grigoropoulos, D. P. Stumbo, J. N. Miller, *Appl. Phys. Lett.* **2008**, *93*, 121116.
[126] Y. Zhang, A. Kolmakov, S. Chretien, H. Metiu, M. Moskovits, *Nano Lett.* **2004**, *4*, 403.
[127] C. H. Wang, X. F. Chu, M. W. Wu, *Sens. Actuators B* **2006**, *113*, 320.
[128] J. Kong, M. G. Chapline, H. J. Dai, *Adv. Mater.* **2001**, *13*, 1384.
[129] A. Kolmakov, D. O. Klenov, Y. Lilach, S. Stemmer, M. Moskovits, *Nano Lett.* **2005**, *5*, 667.
[130] V. V. Sysoev, B. K. Button, K. Wepsiec, S. Dmitriev, A. Kolmakov, *Nano Lett.* **2006**, *6*, 1584.
[131] G. F. Zheng, F. Patolsky, Y. Cui, W. U. Wang, C. M. Lieber, *Nat. Biotechnol.* **2005**, *23*, 1294.
[132] Q. F. Pengfei, O. Vermesh, M. Grecu, A. Javey, O. Wang, H. J. Dai, S. Peng, K. J. Cho, *Nano Lett.* **2003**, *3*, 347.
[133] C. Soci, A. Zhang, B. Xiang, S. A. Dayeh, D. P. R. Aplin, J. Park, X. Y. Bao, Y. H. Lo, D. Wang, *Nano Lett.* **2007**, *7*, 1003.
[134] J. S. Jie, W. J. Zhang, Y. Jiang, X. M. Meng, Y. Q. Li, S. T. Lee, **2006**, *Nano Lett.* **2006**, *6*, 1887.

© 2009 WILEY-VCH Verlag GmbH & Co. KGaA, Weinheim